JOURNAL OF GEOPHYSICAL RESEARCH, VOL. 112, C07017, doi:10.1029/2006JC004039, 2007

Phytoplankton scales of variability in the California Current System: 1. Interannual and cross-shelf variability

Stephanie A. Henson[1] and Andrew C. Thomas[1]

Received 30 November 2006; revised 23 March 2007; accepted 8 May 2007; published 14 July 2007.

[1] In the California Current System, strong mesoscale variability associated with eddies and meanders of the coastal jet play an important role in the biological productivity of the area. To assess the dominant timescales of variability, a wavelet analysis is applied to almost nine years (October 1997 to July 2006) of 1-km-resolution, 5-day-averaged, Sea-viewing Wide Field-of-view Sensor (SeaWiFS) chlorophyll *a* (chl *a*) concentration data. The dominant periods of chlorophyll variance, and how these change in time, are quantified as a function of distance offshore. The maximum variance in chlorophyll occurs with a period of ~100–200 days. A seasonal cycle in the timing of peak variance is revealed, with maxima in spring/summer close to shore (20 km) and in autumn/winter 200 km offshore. Interannual variability in the magnitude of chlorophyll variance shows maxima in 1999, 2001, 2002, and 2005. There is a very strong out-of-phase correspondence between the time series of chlorophyll variance and the Pacific Decadal Oscillation (PDO) index. We hypothesize that positive PDO conditions, which reflect weak winds and poor upwelling conditions, result in reduced mesoscale variability in the coastal region, and a subsequent decrease in chlorophyll variance. Although the chlorophyll variance responds to basin-scale forcing, chlorophyll biomass does not necessarily correspond to the phase of the PDO, suggesting that it is influenced more by local-scale processes. The mesoscale variability in the system may be as important as the chl *a* biomass in determining the potential productivity of higher trophic levels.

Citation: Henson, S. A., and A. C. Thomas (2007), Phytoplankton scales of variability in the California Current System: 1. Interannual and cross-shelf variability, *J. Geophys. Res.*, *112*, C07017, doi:10.1029/2006JC004039.

1. Introduction

[2] The California Current System (CCS) is an eastern boundary flow that originates in the vicinity of British Columbia and extends southward to Baja California. Currents are generally equatorward in summer, and both zonal extent and strength varies seasonally [*Hickey*, 1998]. Instabilities in the mean southward flow produce meanders and eddies around the core of the coastal jet [e.g., *Marchesiello et al.*, 2003]. Mesoscale activity becomes more pronounced as the jet intensifies during spring, before propagating offshore during autumn [*Strub and James*, 2000]. The existence of an energetic eddy field has been extensively documented in hydrographic measurements [e.g., *Kosro*, 1987; *Lynn and Simpson*, 1987; *Huyer et al.*, 1998; *Soto-Mardones et al.*, 2004; *Barth et al.*, 2005]. Moored current meters reveal the dominance of eddy variability [e.g., *Kelly et al.*, 1998], with more than half of the variability in the current ascribed to eddy activity [*Rienecker and Mooers*, 1988]. The high spatial and temporal resolution of satellite data has also been exploited to investigate the region's mesoscale variability in sea surface height, sea surface temperature (SST) and phytoplankton pigment data [e.g., *Abbott and Zion*, 1985; *Strub and James*, 1995, 2000]. Persistent and seasonally recurring mesoscale structure observed in SST and CZCS (Coastal Zone Color Scanner) imagery is often associated with features of the coastal topography and spatial variations in wind-forcing [*Ikeda and Emery*, 1984; *Kelly*, 1985; *Abbott and Barksdale*, 1991].

[3] The impact of mesoscale variability on biological processes has been frequently demonstrated in the CCS. Meanders and eddies have been shown to increase chlorophyll concentrations, either by supplying new nutrients or through physical accumulation of biomass [*Hayward and Mantyla*, 1990; *Chavez et al.*, 1991; *Hood et al.*, 1991; *Abbott and Letelier*, 1998]. This effect is passed up the food chain, with increased zooplankton populations, sardine larvae and even cetaceans associated with eddies [*Huntley et al.*, 1995; *Logerwell and Smith*, 2001; *Tynan et al.*, 2005]. Spectral analysis of SST and CZCS data suggests that phytoplankton behave as passive tracers of the circulation at timescales of a few days to weeks [*Smith et al.*, 1998; *Denman and Abbott*, 1994]. Thus interannual variability in physical forcing may affect not only total phytoplankton biomass, but also its time and space distribution, both of which could impact higher trophic level productivity.

[4] Mesoscale variability is a key characteristic of the CCS ecosystem, but determining the scales at which it occurs, and its interannual and spatial distribution, remains

[1]School of Marine Sciences, University of Maine, Orono, Maine, USA.

0148-0227/07/2006JC004039$09.00

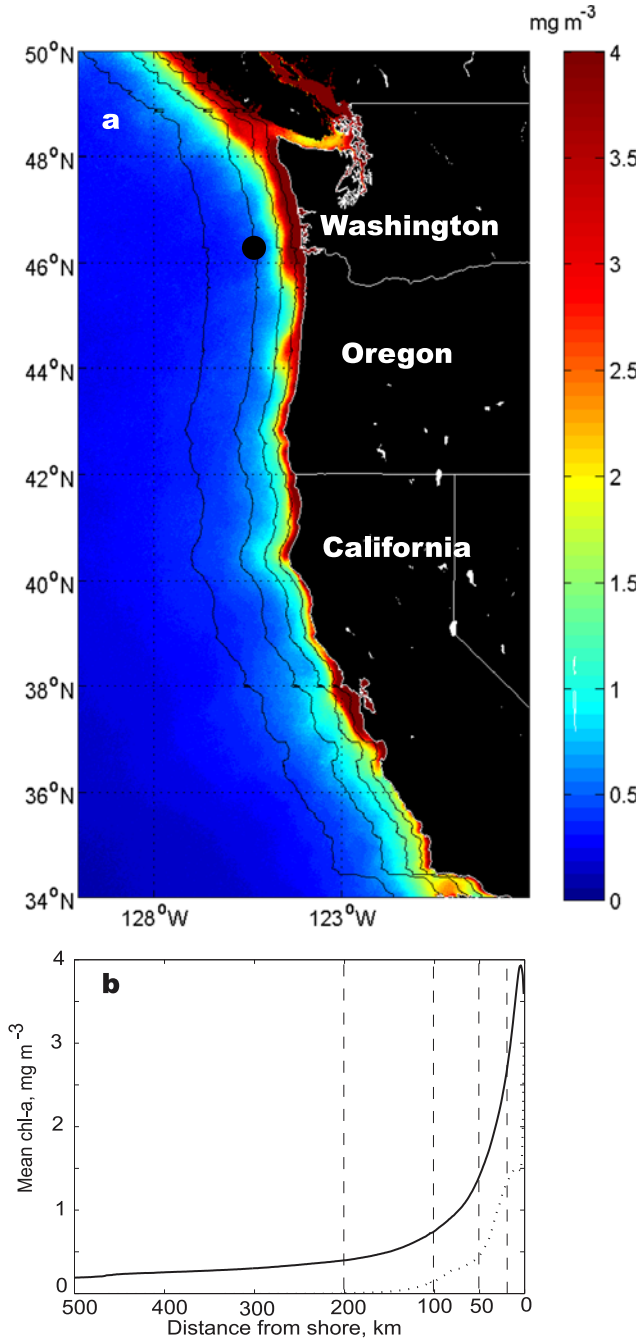

Figure 1. (a) The California Current study region, showing mean SeaWiFS chl *a* (mg m^{-3}) for October 1997 to July 2006. Solid lines mark positions of transects taken 20, 50, 100, and 200 km offshore. Black dot marks position of example time series in Figure 2a. (b) Latitudinally averaged chl *a* concentration (solid line) and variance (dotted line) plotted as a function of distance offshore. Vertical dashed lines mark position of transects.

a challenge. A method commonly employed to identify the dominant frequencies in a time series of data is the Fourier transform. However, the Fourier transform retains no information on the temporal evolution of a signal's spectral characteristics. The wavelet transform (WT) decomposes a signal into time-frequency space, quantifying not only the dominant modes of variability, but also how they vary in time. The WT is increasingly used in geophysical applications to study, for example, Rossby waves in satellite altimetry data [*Cromwell*, 2001; *Charria et al.*, 2006], paleoclimate variability captured in deep-sea sediment records [*Lau and Weng*, 1995], spatial and seasonal variability in satellite chlorophyll data [*Machu et al.*, 1999; *Nezlin and Li*, 2003] and El Niño–Southern Oscillation sea surface temperature signals [*Wang and Wang*, 1996; *Torrence and Compo*, 1998].

[5] Long time series of high-resolution satellite data are now available, but can be so voluminous, with several years of data, often with millions of pixels, and both time and space dimensions to consider, that trying to determine the signals contained therein can be a daunting task. However, these data are well suited to analysis with the WT, as it requires a long (relative to the sampling frequency) time/space series. Our aim in this paper is to characterize the temporal variance in SeaWiFS chlorophyll concentration data in the CCS by identifying the dominant frequencies and examining their interannual and cross-shelf variability. The spatial variability of chlorophyll concentration is considered in a companion paper [*Henson and Thomas*, 2007a]. In section 2 we illustrate the WT method with an example chlorophyll *a* time series, focusing on interpretation of the output, rather than detailed mathematics. In section 3 we present the results of the wavelet analysis with little discussion of the mechanisms behind our observations, which we leave to section 4, where we also place our results in the context of previous work.

2. Methods

2.1. Data

[6] SeaWiFS chlorophyll *a* (chl *a*) concentration data at 1 km resolution were obtained from the NASA Ocean Color Browser (http://oceancolor.gsfc.nasa.gov/). All level 2 MLAC files (v5.1 reprocessing) from 2 October 1997 to 31 July 2006 in the boundaries 34°N–50°N, 130°W–118°W were downloaded (Figure 1a shows a map of the study region). Individual passes were remapped to a cylindrical projection and multiple passes on a calendar day were composited. On average ~20% of the data were missing owing to cloudiness, and therefore daily images were then composited into 5-day means to reduce gaps. Remaining gaps greater than three time steps (i.e., 15 days) in length were filled with a mean value, calculated for that pixel and day of year from all good data in other years. Any gaps shorter than three time steps were filled by linear interpolation in time. The climatological mean seasonal cycle of chl *a* at each location was removed from the data prior to performing wavelet analysis.

2.2. Wavelet Analysis

[7] Our description of wavelet analysis focuses on interpretation of results. Readers interested in the mathematical derivation of WT are referred to *Morlet* [1983] or *Daubechies* [1992]. We illustrate the method, and compare it to Fourier analysis, using a time series of SeaWiFS chl *a* at 46.5°N, 124°W (~100 km offshore; see Figure 1a). The time series of seasonal anomalies at this point (Figure 2a) clearly has periodicities which vary in amplitude interannually.

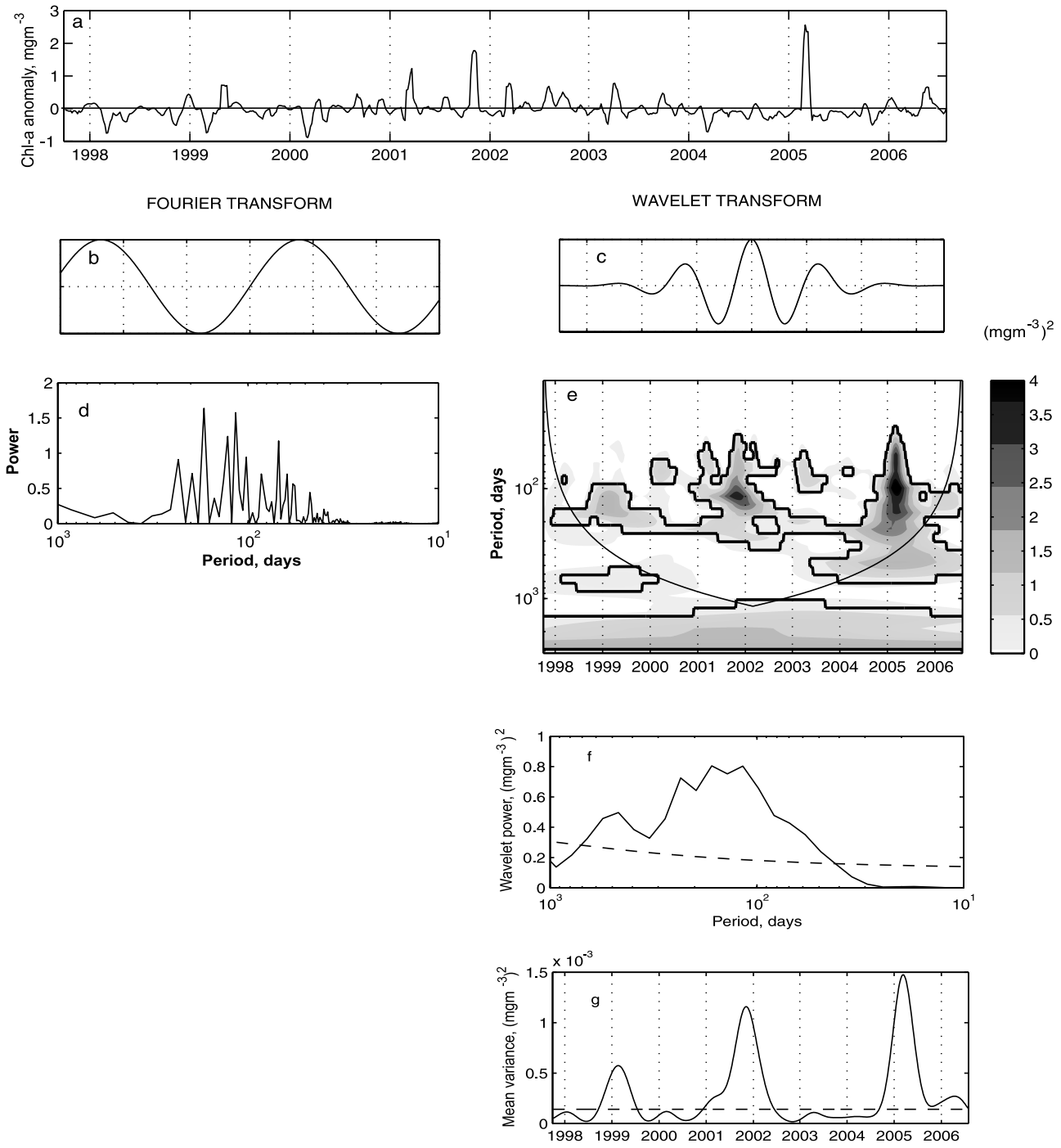

Figure 2. Comparison of Fourier transform and wavelet transform for an example time series. (a) Time series of SeaWiFS chl *a* anomalies at 46.5°N, 124°W. (b) A sine wave, the basis of the Fourier transform. (c) The Morlet-6 wavelet, used for all analysis in this paper. (d) Fourier power spectrum of the time series. (e) Local wavelet power spectrum of the time series. High values of wavelet power indicate frequencies and times at which chl *a* variance is high. Thick black line is the 95% confidence level. Thin line is the cone of influence, below which edge effects become important. The *y* axis has been converted from wavelet scale, *a*, to frequency. For the Morlet-6 wavelet, frequency = 1.03*a* [*Torrence and Compo*, 1998]. The smallest scale resolved is at the Nyquist frequency (~10 days) and the largest is the length of the time series (~3200 days). (f) Global wavelet power spectrum, i.e., the mean wavelet power at each period. Dashed line is the 95% confidence level. (g) Scale-averaged time series for the period band 100–140 days. Wavelet power has been normalized by $N/2\sigma^2$ (where N is the number of data points and σ^2 is its variance). Dashed line is the 95% confidence level.

[8] A Fourier transform breaks down the signal into a series of sine and cosine waves (e.g., Figure 2b) with various frequencies. The resulting Fourier power spectrum of the data (Figure 2d) has several peaks with periods of 100–200 days, with maxima at periods of 116 and 170 days. However, the Fourier spectrum provides no information on how the dominant periods may vary with time over the sampling period. The WT decomposes the signal into a series of wavelets, which are stretched and shifted versions of the original (or mother) wavelet (Figure 2c). Mother wavelets must have a zero mean and be localized in both time and frequency space (unlike sinusoids which extend from minus to plus infinity). The WT of a time series is defined as

$$W(b,a) = \frac{1}{\sqrt{a}} \int \psi\left(\frac{t-b}{a}\right) f(t)dt, \quad (1)$$

where ψ is the mother wavelet. The parameters a and b determine the shape and location of the wavelets. Changing a stretches or compresses the wavelet to encompass different frequencies, while changing b moves the centre of the wavelet in time, so that the WT can be applied to all data points in a time series. The wavelet transform, W, is then a 2-D matrix describing the relative amplitude of features at a particular frequency and time. (Note that formally a is the wavelet scale, not frequency, although there is a close correspondence between the two [*Meyers et al.*, 1993]).

[9] As a mother wavelet we selected the Morlet wavelet (with nondimensional frequency = 6), commonly used in geophysical applications because of its good frequency localization (Figure 2c). Applying the WT to the chl *a* time series (Figure 2a) yields the local wavelet power spectrum (LWPS), defined as $|W(b, a)|^2$, plotted in Figure 2e. The unit of wavelet power is the original data unit squared, i.e., the variance (in the case of chl *a* this is (mg m^{-3})^2). Thick solid lines denote the 95% confidence level, assuming a white-noise background spectrum (a detailed derivation of the confidence level calculations is given by *Torrence and Compo* [1998]). Errors increase at the edges of the wavelet spectrum because of the finite length of the time series, and data below the cone of influence (thin solid line in Figure 2e) should be regarded with caution. The contours represent wavelet power and can be interpreted as a 'map' of the time variability of dominant frequencies. The largest peak in wavelet power occurs in early 2005, with a period of 30–150 days. Another peak occurs in autumn 2001, with a dominant period of 100–110 days. In the other years, statistically significant variability occurs in a band with periods of ~100–200 days. For interpretation, recall that the WT is not detecting an increase or decrease in the absolute magnitude of the data, but rather an increase or decrease in the variance of the data.

[10] The information contained in the local wavelet spectrum can be summarized by the global wavelet power spectrum (GWPS; Figure 2f) and scale-averaged time series (Figure 2g). The GWPS is the time-averaged wavelet power at each period and is equivalent to the frequency-smoothed Fourier power spectrum in Figure 2d. The mean wavelet power has a broad peak with periods between ~100 and 200 days, with a maximum at 116 days (Figure 2f). The scale-averaged time series is the mean variance contained in a certain period band. Averaging over the period band 100–140 days (Figure 2g) indicates that maximum variance occurs in early spring 1999, late 2001 and early in 2005. In the other years the variance in this period band is below the 95% confidence level.

[11] The example WT in Figure 2 was performed at a point location 100 km off the Washington coast, but wavelet analysis can be extended to analyze the latitudinal and zonal variations in the dominant scales of variability and how they vary interannually. To quantify the dominant timescales of variability, wavelet analysis was performed on transects of SeaWiFS chl *a* taken at fixed distances offshore (20, 50, 100 and 200 km) and averaged latitudinally over the entire range from 34°N–50°N.

3. Results

[12] A map of the time series mean chl *a* in the study region, with the positions of the offshore transects marked, is shown in Figure 1a. The 20 km transect encounters the highest chl *a* concentrations, which are located in a relatively narrow band close to shore. The offshore extent of high chl *a* (red colors) is widest north of ~48°N, and is crossed by the 50 km transect which otherwise borders the edge of the inshore chl *a* maximum. The 100 km transect crosses regions of intermediate chl *a* concentration, with the exception of north of ~48°N. The 200 km transect encounters almost uniformly low chl *a*. We do not venture closer to shore than 20 km, as the SeaWiFS data here are potentially influenced by resuspension and terrestrial and freshwater runoff products, leading to spurious chl *a* values. Transects greater than 200 km offshore are not presented as waters become oligotrophic and hence variance is very low. The rapid offshore decrease in chl *a* concentration is illustrated in Figure 1b which shows the latitudinally averaged climatological mean chl *a* as a function of distance offshore. Within the first 50 km of the coast the mean chl *a* decreases by half. The variance also decreases rapidly offshore and by 200 km offshore is nearly zero. The locations of the transects we have selected therefore capture the majority of the offshore extent of increased chl *a* concentrations in the CCS. The results of the wavelet analysis performed at each of the four distances offshore are shown as contour plots of the local wavelet power spectra in Figures 3a–3d. Global wavelet power spectra (Figures 3e–3h) and scale-averaged time series (Figure 4) for each transect are also plotted.

3.1. Twenty Kilometers Offshore

[13] Peaks in wavelet power generally occur in spring/summer of each year with a dominant period of ~100–

Figure 3. Local wavelet power spectra (mg m^{-3})^2 for temporal analysis of transects (a) 20 km, (b) 50 km, (c) 100 km, and (d) 200 km offshore. Thick lines indicate 95% confidence level. Thin lines mark the cone of influence below which edge effects become important. Global wavelet power spectra (mg m^{-3})^2 for transects (e) 20 km, (f) 50 km, (g) 100 km, and (h) 200 km offshore. Dashed lines indicate 95% confidence level.

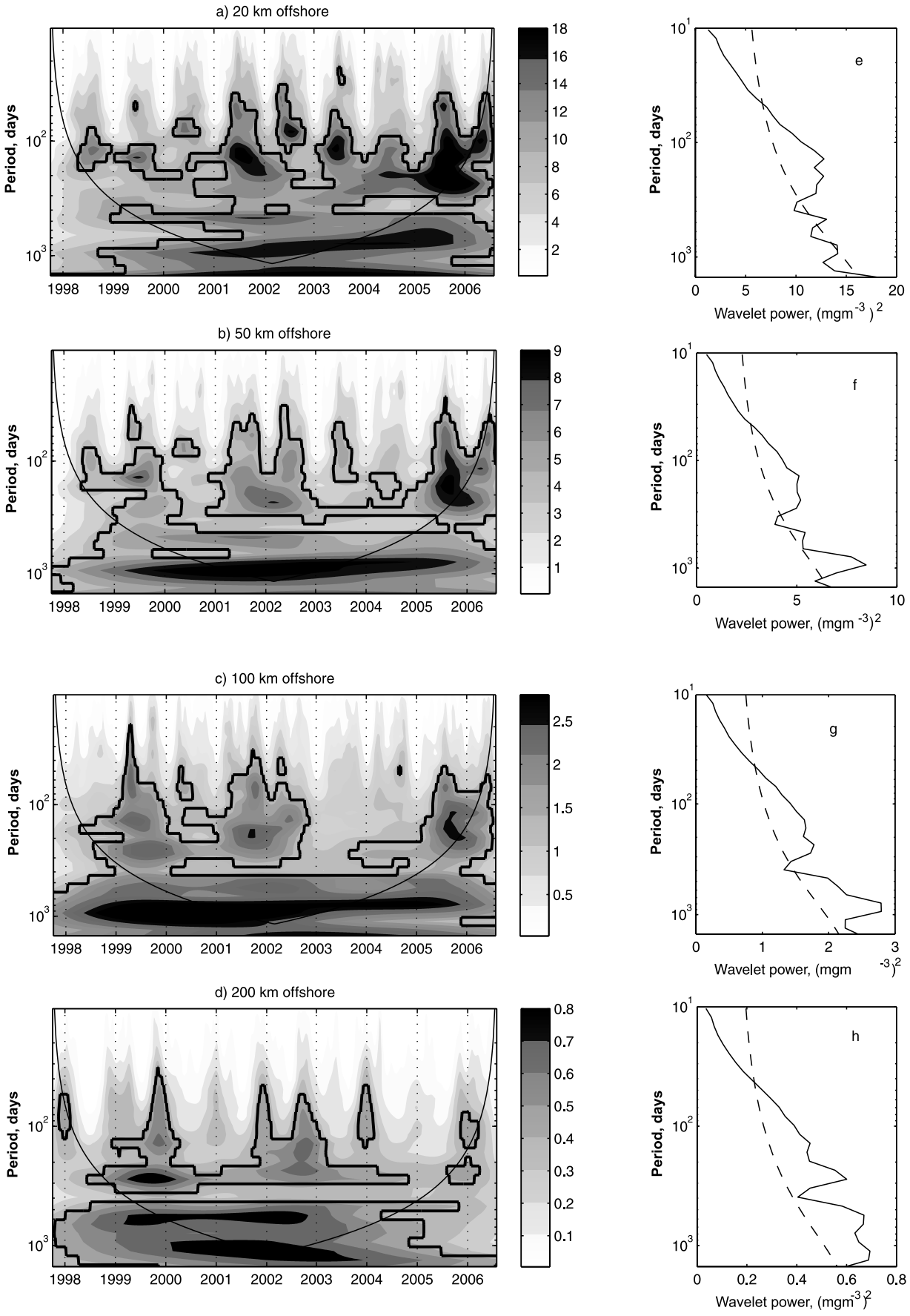
a) 20 km offshore
b) 50 km offshore
c) 100 km offshore
d) 200 km offshore
Period, days
1998 1999 2000 2001 2002 2003 2004 2005 2006
e
f
g
h
Wavelet power, (mgm-3)2

Figure 3

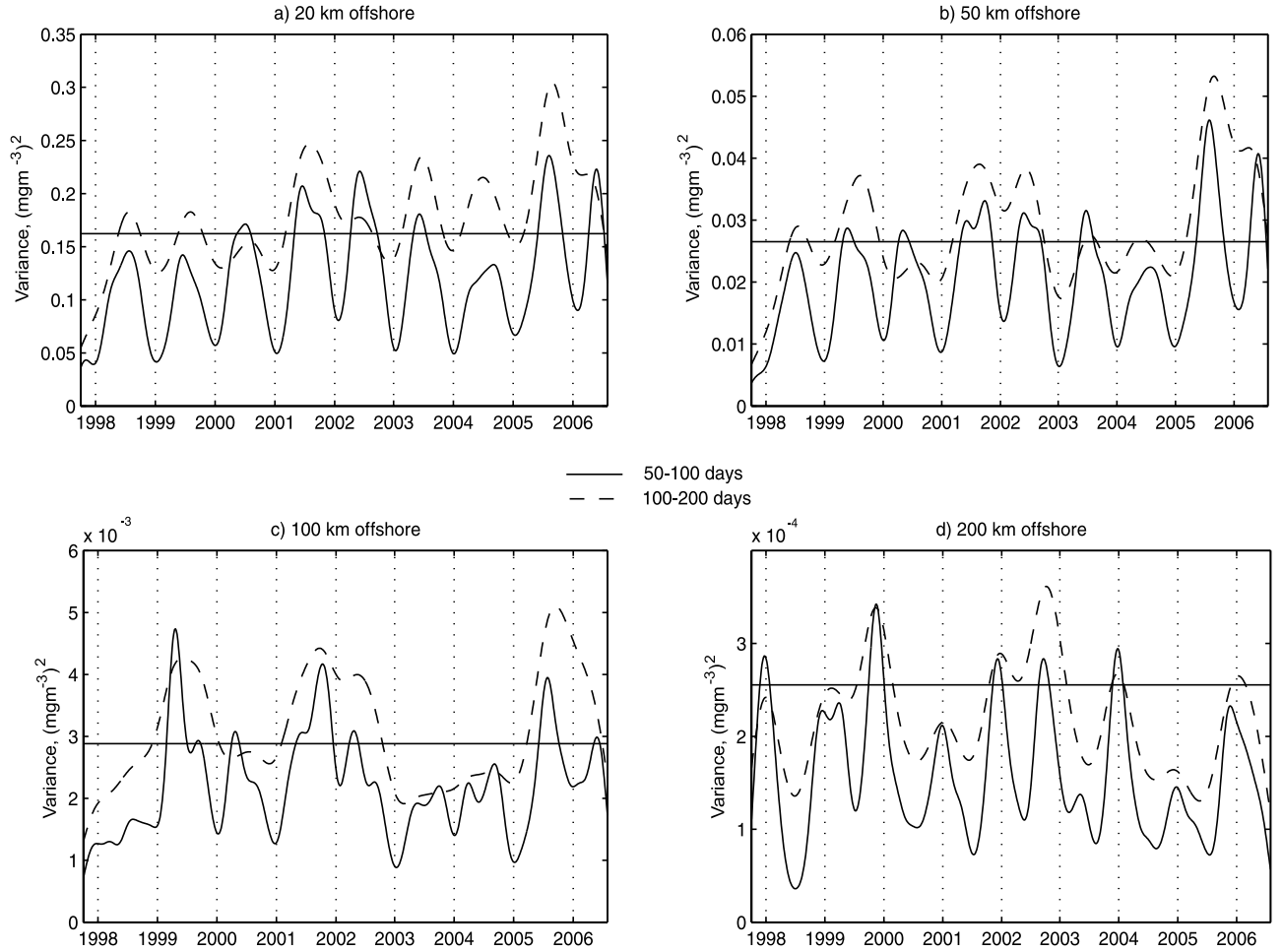

Figure 4. Scale-averaged time series variance (mg m^{-3})^2 in period bands 50–100 (solid line) and 100–200 (dashed line) days for transects (a) 20 km, (b) 50 km, (c) 100 km, and (d) 200 km offshore. Solid horizontal lines mark the 95% significance level. Note that edge effects reduce the wavelet power at the beginning and end of the time series.

200 days (Figure 3a). The shortest significant periods resolved 20 km offshore are ~30 days (thick black line in Figure 3a). The GWPS of the wavelet analysis (Figure 3e) demonstrates that the power at this period is barely significant globally. (Note that wavelet power in a particular period band can be less than significant globally, but still have significant peaks locally [*Torrence and Compo*, 1998]). At periods less than ~50 days wavelet power is at its minimum and not significantly greater than the equivalent white noise spectrum. Wavelet power steadily increases to a maximum at a period of ~140 days, with a second peak at ~200 days. The GWPS has further peaks at ~460 and 800 days, although these are barely significant. At these long periods edge effects become influential and the results should be viewed with caution. While the GWPS illustrates the mean pattern of wavelet power, examination of the local wavelet power spectrum (Figure 3a) allows the distribution of power in time to be investigated. The dominant pattern is a strong seasonality with maximum (minimum) variability in summer (winter), extending to shorter timescales in summer. In 2002 the dominant variance occurs at noticeably shorter periods (~50–100 days) than in other years (~100–200 days).

[14] The scale-averaged time series 20 km offshore (Figure 4a) assists in highlighting the interannual differences in wavelet power. The power is averaged in two period bands, 50–100 and 100–200 days, and normalized to variance. In all years the variance decreases sharply in winter, increasing again in spring. In the period band 50–100 days variance is weakest in 1998, 1999 and 2004, with peaks below the 95% significance level, as they are in the LWPS. In 2001, a broad double-maximum peak is statistically significant. In the 100- to 200-day period band (Figure 4a), all years except 2000 have peaks which are significant. Weakest variance occurs in 2000 and intermediate levels of variance in 1998, 1999 and 2002. High chl *a* variance is found in 2001, 2003 and 2004. Maximum wavelet power in the almost 9-year time series occurs in early September 2005. In 2001/2002 variance remains significant throughout the winter. In all other years variance drops below the significance level in winter (although not as sharply as for the 50- to 100-day band).

[15] In summary, at 20 km offshore weak variance occurs in 1998, 1999 and 2000, with 2000 having the least wavelet power. Strong variance occurs in 2001–2004, with a maximum in 2005. 1998, 1999, 2001 and 2003 have

maximum power at periods of ~100–150 days, while in 2000 and 2002 shorter-period (~60–100 days) variance dominates.

3.2. Fifty Kilometers Offshore

[16] At 50 km offshore maximum variance occurs in summer at periods of ~100–300 days (Figure 3b). Shortest statistically significant periods are ~30 days. The LWPS has broad peaks in variance in 1999, 2001–2002 and 2005 at periods of ~50–200 days. The GWPS (Figure 3f) has peaks at periods of ~140 and 230 days. Interannual variability highlighted by the scale-averaged time series (Figure 4b) shows weakest (below significance level) variance in 1998 and 2004 in the 50- to 100-day period band. Years 1999, 2000 and 2003 have similar variances with peaks in spring/summer (although they are barely statistically significant). Highest variance in this period band occurs in 2001 and 2002, maximum in 2005. In 2001 a double peak (in early summer and late winter) is well defined (compare to Figure 4a), and there is also a suggestion of this seasonal pattern in 1999, 2002 and 2003. In the 100- to 200-day band, variance in 2000 is not significant. Years 1998, 2003 and 2004 have similar magnitude variances, which are barely significant. High variance occurs in 1999, 2001 and 2002 with maximum variance in this period band in 2005. In several years, the peak in the 100- to 200-day band occurs later in the year than that of the 50- to 100-day band.

3.3. One Hundred Kilometers Offshore

[17] At 100 km offshore, strong interannual variability in wavelet power occurs, with the dominant periods at ~60–200 days (Figure 3c). The LWPS has broad peaks in variance in 1999, 2001–2002 and 2005 at periods of ~50–200 days. In other years there is very little variance at any period. Peaks in the GWPS occur at ~140 and 230 days (Figure 3g). The scale-averaged time series in the 50- to 100-day period band (Figure 4c) show that 1998, 2003 and 2004 have less than significant variance. Variance in 2000 and 2002 is barely significant, but 1999, 2001 and 2005 have strong peaks. The double peak in variance is clearly defined in all years, except 2005, but only occurs in the shorter-period band. In the 100- to 200-day period band there are no double peaks within a season. Maximum chl *a* variance occurs in 1999, 2001–2002 and 2005. In other years variance is below the significance level.

3.4. Two Hundred Kilometers Offshore

[18] At 200 km offshore, the peaks in wavelet power occur in autumn/winter of each year, in contrast to spring/summer closer to shore (Figure 3d). The GWPS has peaks at ~140 and 280 days (Figure 3h). The LWPS shows a background of significant power at ~200–300 days (Figure 3d). In all years, with the exception of winter 2004/2005, power occurs at periods of ~30–160 days. The scale-averaged time series (Figure 4d) shows that in all years maximum variance occurs in winter. In the period band 50–100 days the winter variance is weakest in 2004/2005 and below the significance level in 1998/1999, 2000/2001 and 2005/2006. In winter 1999/2000 a double peak occurs with maxima at the end of November 1999 and the end of March 2000. In the 100- to 200-day period band, maximum variance again occurs in winter of each year, and has a similar interannual distribution as the 50- to 100-day period band. Maximum variance occurs in winter 1999/2000, 2001/2002 and 2002/2003.

4. Discussion

[19] The results of the wavelet analysis presented here have the potential to offer a unique view on the scales of variability in the phytoplankton population of the California Current System. While the time/space patterns of mesoscale variability of several physical parameters in the CCS, such as sea surface height and temperature have been reported [e.g., *Strub and James*, 2000; *Kelly et al.*, 1998], the biological response is less well understood. This is partly due to the difficulty in synoptically resolving small space scale and timescale variability in oceanographic cruise data, and even greater difficulty in collecting interannual data sets. Applying wavelet analysis to the high-resolution, multiyear SeaWiFS chl *a* data set allows insight into the dominant scales of variability, and how they vary in time.

4.1. Dominant Timescales

[20] Our results show maximum variance in the SeaWiFS chl *a* data associated with periods of ~100–200 days (Figure 3), with shorter periods tending to occur closer to shore (<100 km). Note that although the smallest resolvable period is theoretically at the Nyquist frequency (i.e., ~10 days), the shortest statistically significant periods are ~30 days. Performing the WT on daily data may resolve smaller-scale processes, but missing data due to cloud cover would probably make the analysis impractical. Indeed, *Chelton and Schlax* [1991] demonstrate that for CZCS data in the CCS, processes with timescales shorter than ~10 days cannot be statistically resolved owing to cloud gaps.

[21] Previous publications have tended to focus on very short timescale variability in chlorophyll concentration, investigated using Fourier spectra; hours to days in the case of drifters and moorings, and two to several days in short, cloud-free sequences of satellite-derived data [*Denman and Abbott*, 1994; *Abbott et al.*, 1995; *Abbott and Letelier*, 1998]. At seasonal timescales, wavelet analysis of SeaWiFS chl *a* for a point location in the Santa Monica Basin concluded that periods of ~66 days dominated, with periods <100 days typically occurring in spring [*Nezlin and Li*, 2003]. *Chelton and Schlax* [1991] show a Fourier analysis of chlorophyll data taken off Scripp's pier with a peak at ~50–60 days. Spectral analysis performed on SeaWiFS chl *a* data from the Gulf of California showed a peak at ~30 days [*Kahru et al.*, 2004], which the authors attribute to tidal forcing. Shorter-period oscillations (~20 days) were found to occur in simulated chlorophyll during summer in a modeling study of the Oregon shelf [*Spitz et al.*, 2005].

[22] Although mesoscale variability in the CCS has been frequently observed [e.g., *Ikeda and Emery*, 1984; *Abbott and Barksdale*, 1991; *Barth et al.*, 2005], reports of the dominant timescales are relatively sparse. The mesoscale variability is estimated to have periods of 100–150 days from moored current data and altimeter-derived surface velocities (*Kelly et al.* [1998] and *Strub et al.* [1997], respectively). Results from an array of current meters moored near Point Arena found a reduction in the dominant period of eddy kinetic energy from 60 days nearshore to

120–180 days ~600 km offshore [*Chereskin et al.*, 2000]. Analysis of eddy kinetic energy estimated from RAFOS floats indicated 'wave-like' structures with periodicities of 100–120 days [*Collins et al.*, 2004]. We note here the matching of scales between the observed mesoscale physical variability and the dominant period of chl *a* variance in the CCS.

4.2. Seasonal Variability

[23] Our results demonstrate that maximum variance occurs in spring/summer at the inshore locations (20, 50 and 100 km offshore), but shifts to autumn/winter seaward of 100 km (Figures 3 and 4). The wavelet analysis was repeated for several more transects (not shown) at various distances offshore (4, 10, 30, 150, 300 and 400 km), which confirmed the seasonal progression in the timing of the peak chl *a* variance. This seasonality is consistent with previous views of the seasonal dynamics and distribution of chl *a* biomass in the region. *Strub and James* [2000] used a combination of satellite altimeter, sea surface temperature (SST) and ocean color (CZCS) data to study the seasonal evolution of the CCS circulation. Their results show that the southward flowing Californian coastal jet forms close to the coast (<200 km) in spring, but by summer is starting to diffuse and has migrated ~100–300 km from shore. In autumn and winter the jet begins to dissipate energy and moves even farther offshore. Eddy variance next to the coast increases in spring, but at the same time reaches a seasonal minimum offshore. High chlorophyll concentrations occur inshore of the jet, and as the jet moves offshore in autumn, so do the elevated chlorophyll levels [*Strub and James*, 2000]. Surface measurements of temperature and salinity taken during two cruises conducted in spring and summer 2001 off the Oregon coast confirmed that the core of the jet lay nearshore during spring, moving offshore during summer [*Castelao and Barth*, 2005]. Eddy kinetic energy derived from RAFOS float measurements in the vicinity of Point Arena also demonstrates a seasonal movement of the jet [*Collins et al.*, 2004]. Peak jet velocities were observed close to shore (<85 km) in May, but greater than 400 km offshore in October. *Collins et al.* [2004] associated the decay of the jet in autumn with the development of eddies and meanders. Interestingly, they also show that along-shore jet velocity has a double peak in May and December in their 'transition zone' (~100 km offshore; compare to Figure 4c). A double peak in the seasonal cross-shelf extension of high chlorophyll concentration was also noted in CZCS data in the northern CCS [*Thomas and Strub*, 2001]. The seasonal offshore migration of the eddy kinetic energy associated with the coastal jet has been observed in regional modeling studies [*Haney et al.*, 2001; *Marchesiello et al.*, 2003]. Our results are consistent with this view of the seasonal changes in cross-shelf patterns of the jet's physical structure. We have demonstrated that there is also a biological signature associated with the seasonal migration of the coastal jet. Both the timing of the jet's offshore movement, and the dissipation of energy associated with it, are reflected in the results of the wavelet analysis.

4.3. Interannual Variability

[24] Substantial interannual variability is apparent in the results of the wavelet analysis. Away from the immediate vicinity of the shore (>20 km offshore) 1998, 2000, 2003 and 2004 evinced lower chl *a* variance than the other study years (Figures 3 and 4). Years 1999, 2001, 2002 and 2005 consistently display the greatest chl *a* variance in both period bands presented. What processes could result in the interannual variability observed in the chl *a* data? Previous work in the CCS suggests a close coupling between time/space patterns of phytoplankton variability and physical processes that affect the intensity of coastal upwelling. At the scales resolved here, the patterns of chl *a* distribution will be affected by, among other factors, lateral and vertical mixing, currents, wind-forcing, nutrient availability and grazing pressure. In the CCS specifically, the onset of southward (i.e., upwelling favorable) winds in spring and the subsequent upwelling strength will be important factors in determining the magnitude and distribution of chl *a* [*Thomas and Strub*, 1989, 2001; *Abbott and Barksdale*, 1991]. The southward flowing coastal jet, interacting with the topography of the CCS, develops numerous mesoscale features during the spring and summer [*Ikeda and Emery*, 1984; *Haidvogel et al.*, 1991; *Barth et al.*, 2000; *Marchesiello et al.*, 2003], which influence the cross-shelf distribution of chl *a* [e.g., *Hood et al.*, 1990]. The intensity and position of the coastal jet is likely to contribute to the variance in the chl *a* signal. Superimposed on these local effects, basin-scale processes, such as El Niño/La Niña events, also impact the biological productivity of the CCS by altering wind patterns and upwelling intensity [e.g., *Lynn et al.*, 1998]. In addition to these physical processes, biological factors, such as growth, decay and grazing could also introduce variance, so that chl *a* may not be merely a passive tracer of physical forcing in the CCS.

[25] The wavelet analysis shows that chl *a* variance in 1998 is much reduced up to ~100 km offshore. Shorter-period variance (50–100 days) is particularly affected and is not statistically significant at any location (Figure 4). Chl *a* variance in 2003 and 2004 is also generally weak and often not statistically significant. A strong El Niño (EN) occurred in 1997/1998, and weak tropical EN conditions were also present in 2002/2003 and 2003/2004. In the CCS, EN conditions result in warm SST, weak equatorward (i.e., upwelling favorable) winds and a weakening of the coastal jet [*Chelton et al.*, 1982; *Simpson*, 1984a, 1984b; *Lynn et al.*, 1998; *Nezlin and McWilliams*, 2003], consistent with reduced chl *a* variability.

[26] Chl *a* variance in 1999 is strong in both period bands at distances greater than ~50 km offshore (Figure 4). Typical La Niña conditions prevailed in 1999, characterized by cool water conditions, anomalously strong upwelling favorable winds and a more vigorous coastal jet [*Hayward et al.*, 1999; *Schwing et al.*, 2000; *Bograd et al.*, 2000]. Cool water conditions persisted in the CCS from 1999 through 2001 [*Bograd et al.*, 2000; *Durazo et al.*, 2001; *Schwing et al.*, 2002a]. The chl *a* variance might then be expected to be similar in these three years. Indeed 1999 and 2001 are similar, with high variance in both years occurring at all locations (Figure 4). However, in 2000 some of the lowest values of chl *a* variance are observed at all distances offshore. Weaker than usual upwelling was observed in parts of Southern California, but was near normal off Oregon. Chl *a* concentrations were lower than in 1999, but near the climatological mean [*Durazo et al.*, 2001].

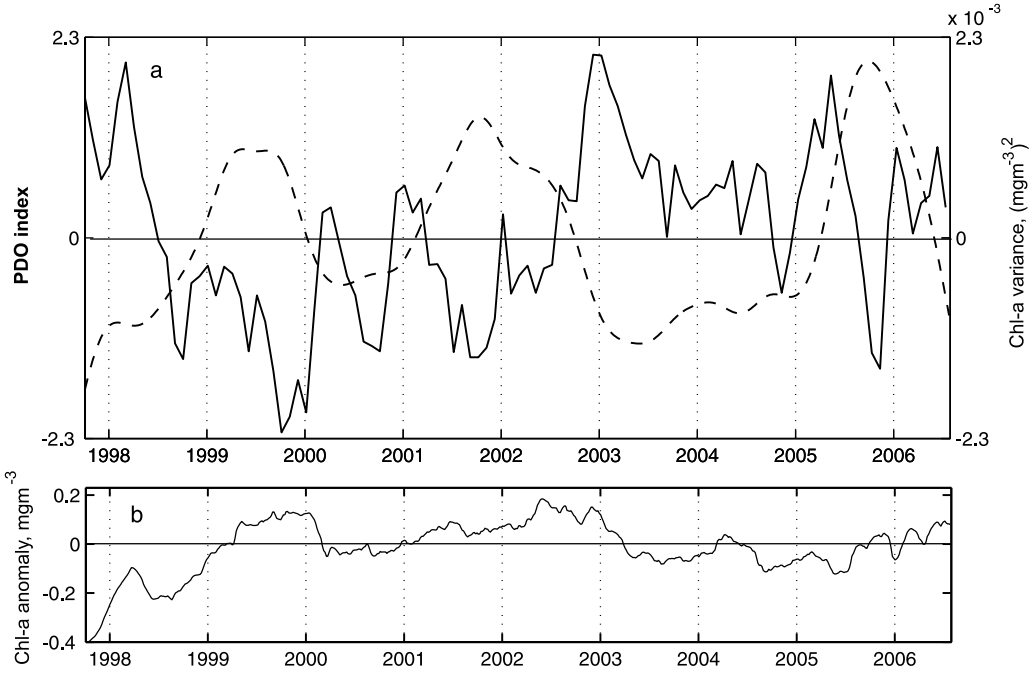

Figure 5. (a) Pacific Decadal Oscillation (solid line) and SeaWiFS chl *a* variance 100 km offshore in the 100- to 200-day period band (dashed line). The annual harmonic component of the chl *a* variance has been removed to highlight the interannual variability. (b) Chl *a* concentration anomalies (climatological mean seasonal cycle removed) 100 km offshore.

[27] Unusually strong upwelling conditions occurred through 2001 and 2002, and southward flow may have continued intermittently during the winter of 2001/2002 [*Venrick et al.*, 2003]. An anomalous mass of cold, nutrient-rich, subarctic water was observed on the shelf in 2002, stretching from British Columbia to Southern California [*Bograd and Lynn*, 2003], resulting in higher than normal chl *a* concentrations [*Wheeler et al.*, 2003; *Thomas et al.*, 2003]. The velocity of the coastal jet was also faster than usual in 2002 [*Kosro*, 2003; *Barth*, 2003]. The WA shows continued high chl *a* variance in winter 2001/2002 compared to other years. Strong chl *a* variance occurs in 2002 at all offshore locations. The dominant period of chl *a* variance is also shorter in the nearshore region (>50 km offshore) in 2002 than in other years (Figures 3a and 3b).

[28] The WA identifies very strong variance in chl *a* in 2005 in both period bands at the three locations closest to shore (Figure 4). This variance is associated with known anomalous conditions in 2005. SeaWiFS chlorophyll images show that the spring bloom in the northern CCS had a brief (~3 week long), and anomalously early, peak in February which quickly receded. A sustained increase in biomass did not occur again until early July [*Thomas and Brickley*, 2006; *Henson and Thomas*, 2007b]. The onset of upwelling favorable winds and an equatorward coastal jet were delayed until late May in 2005 [*Kosro et al.*, 2006]. Once upwelling conditions were finally established in June, unusually strong equatorward winds and vigorous upwelling persisted until autumn [*Schwing et al.*, 2006].

[29] Interannual variability in climatic conditions in the Northeast Pacific is represented by several climate indices. The Pacific Decadal Oscillation (PDO) index is based on the leading principal component of North Pacific monthly sea surface temperature variability and reflects large-scale conditions that impact the region on interannual and decadal scales [*Mantua and Hare*, 2002]. In the eastern basin warm period (positive index) PDO indicates high SST, analogous to EN conditions. Reduced biological productivity is also observed in positive PDO phases [*Francis and Hare*, 1994; *Mantua et al.*, 1997; *Pennington et al.*, 2006]. The conditions are reversed in negative periods of the PDO. In Figure 5a the monthly PDO index for October 1997 to July 2006 is plotted (downloaded from http://www.jisao.washington.edu/pdo/). An almost continuously warm PDO period occurs from mid-1997 to mid-1998, and again from mid-2002 to mid-2005. Also plotted in Figure 5a is the chl *a* variance 100 km offshore in the 100- to 200-day period band. This is the same data as in Figure 4c, but the seasonal cycle (annual harmonic component) has been removed to highlight interannual variability. These data show clearly that in positive (negative) PDO periods the chl *a* variance is low (high).

[30] As a linkage between these processes, we hypothesize that the interannual variability in the intensity of the coastal jet contributes to the observed interannual variability in the chl *a* variance. In the CCS, positive PDO conditions imply warm SST, weak equatorward winds, and hence poor upwelling conditions [*Schwing et al.*, 2002b; *Peterson and Schwing*, 2003]. Weaker winds are also associated with a reduced intensity coastal jet and lower southward transport [*Chelton et al.*, 1982; *McGowan et al.*, 1998; *Murphree et al.*, 2003]. The coastal jet is a source of much of the mesoscale variability in the CCS, the meanders, eddies and filaments of which have frequently been documented in satellite imagery [e.g., *Ikeda and Emery*, 1984; *Abbott and Barksdale*, 1991; *Strub and James*, 2000] and in field

data [*Chavez et al.*, 1991; *Soto-Mardones et al.*, 2004; *Castelao et al.*, 2005; *Barth et al.*, 2005]. Years in which strong winds and upwelling occur are likely to have a vigorous coastal jet, which may enhance mesoscale variability in the region. Increased variability in the physical environment is likely to be reflected in enhanced chlorophyll variance.

[31] We contrast the interannual variability in chl *a* variance with that of chl *a* biomass. The time series of chl *a* concentration anomalies (climatological seasonal cycle removed) averaged over the transect 100 km offshore is plotted in Figure 5b. Large negative anomalies occur in 1997/1998 with additional, smaller, anomalies in 2000 and early 2003 to mid 2005. In 1998 to 2000 chl *a* concentration varies out of phase with the PDO index, and in phase with the chl *a* variance. In this period a very strong El Niño event (1997/1998) and subsequent sudden switch to La Niña conditions (1999/2000) occurred. From 2001 onward however, chl *a* concentration no longer covaries with either the PDO or the chl *a* variance. Our observation is that the chl *a* biomass appears to respond to basin-scale forcing, represented by the PDO index, only when anomalous conditions are sufficiently great (as in strong ENSO years) to override local processes. In years when basin-scale forcing is weaker (2001 onward) the biomass is controlled to a greater extent by small-scale, local processes. For example, the intrusion of subarctic water into the northern CCS in 2002 results in large positive chl *a* concentration anomalies, but no corresponding signal is seen in the PDO, suggesting that the event was predominantly driven by local forcing. Although the chl *a* biomass is not well correlated with the PDO, the variance in chl *a* is. This suggests that the processes affecting variance occur at larger scales than those controlling biomass.

[32] The different responses in biomass and variance to large-scale versus local forcing have not previously been noted. Interannual variability in chl *a* variance, as well as biomass, may have significant effects on higher trophic levels. Increased zooplankton volumes [*Huntley et al.*, 1995], sardine survival rates [*Logerwell and Smith*, 2001], juvenile hake catches [*Sakuma and Ralston*, 1997] and even increased density of salmon fishing vessels [*Thomson et al.*, 1992] are associated with eddies in the CCS. It may be that interannual variability in chlorophyll variance is as strong a contributor to variability at higher trophic levels as interannual variability in biomass.

5. Summary

[33] The application of wavelet analysis to the SeaWiFS data set quantifies the temporal scales of variability in chlorophyll concentration in the CCS, and how chl *a* variance changes interannually. The analysis was performed on latitudinal means of chl *a* at distances 20, 50, 100 and 200 km offshore. Variance decreases with distance offshore, although the pattern of interannual variability is similar at all locations. Years 1999, 2001, 2002 and 2005 consistently have the greatest chl *a* variance. The dominant period of variability is ~100–200 days, except in 2002 when shorter periods (50–100 days) dominate. Seasonally, the timing of the peak variance changes with distance offshore, occurring in spring/summer at distances <100 km, but in autumn/winter farther offshore. This is consistent with the seasonal offshore migration of the California coastal jet. Years with high chl *a* variance (1999, 2001, 2002 and 2005) correspond to periods of negative PDO index, which is associated with stronger upwelling and a more vigorous coastal jet. We suggest that this contributes to enhanced variability in the coastal region, which the wavelet analysis detects as increased variance in chl *a*. Chlorophyll biomass, however, does not necessarily correspond to the phase of the PDO, suggesting an increased influence by local-scale, rather than basin-scale, processes. The variance in the CCS may be as important as the chl *a* biomass in assessing the potential productivity of higher trophic levels. A companion paper [*Henson and Thomas*, 2007a] extends the wavelet analysis to examine the latitudinal variability in chlorophyll variance.

[34] **Acknowledgments.** Wavelet software was provided by C. Torrence and G. Compo, and is available at URL: http://paos.colorado.edu/research/wavelets/. SeaWiFS data were provided by GSFC/NASA in accord with the SeaWiFS Research Data Use Terms and Conditions Agreement. This work was funded by NSF grants OCE-0535386 and OCE-0531289 to ACT. This is contribution 525 to the U.S. GLOBEC program.

References

Abbott, M. R., and B. Barksdale (1991), Phytoplankton pigment patterns and wind forcing off central California, *J. Geophys. Res.*, *96*(C8), 14,649–14,667.

Abbott, M. R., and R. M. Letelier (1998), Decorrelation scales of chlorophyll as observed from bio-optical drifters in the California Current, *Deep Sea Res., Part II*, *45*(8–9), 1639–1667.

Abbott, M. R., and P. M. Zion (1985), Satellite observations of phytoplankton variability during an upwelling event, *Cont. Shelf Res.*, *4*(6), 661–680.

Abbott, M. R., K. H. Brink, C. R. Booth, D. Blasco, M. S. Swenson, C. O. Davis, and L. A. Codispoti (1995), Scales of variability of bio-optical properties as observed from near-surface drifters, *J. Geophys. Res.*, *100*(C7), 13,345–13,367.

Barth, J. A. (2003), Anomalous southward advection during 2002 in the northern California Current: Evidence from Lagrangian surface drifters, *Geophys. Res. Lett.*, *30*(15), 8024, doi:10.1029/2003GL017511.

Barth, J. A., S. D. Pierce, and R. L. Smith (2000), A separating coastal upwelling jet at Cape Blanco, Oregon and its connection to the California Current System, *Deep Sea Res., Part II*, *47*(5–6), 783–810.

Barth, J. A., S. D. Pierce, and T. J. Cowles (2005), Mesoscale structure and its seasonal evolution in the northern California Current System, *Deep Sea Res., Part II*, *52*(1–2), 5–28.

Bograd, S. J., and R. Lynn (2003), Long-term variability in the Southern California Current System, *Deep Sea Res., Part II*, *50*(14–16), 2355–2370.

Bograd, S. J., et al. (2000), The state of the California Current, 1999–2000: Forward to a new regime?, *CalCOFI Rep.*, *41*, 26–52.

Castelao, R. M., and J. A. Barth (2005), Coastal ocean response to summer upwelling favorable winds in a region of alongshore bottom topography variations off Oregon, *J. Geophys. Res.*, *110*, C10S04, doi:10.1029/2004JC002409.

Castelao, R. M., J. A. Barth, and T. P. Mavor (2005), Flow-topography interactions in the northern California Current System observed from geostationary satellite data, *Geophys. Res. Lett.*, *32*(24), L24612, doi:10.1029/2005GL024401.

Charria, G., I. Dadou, P. Cipollini, M. Drevillon, P. De Mey, and V. Garcon (2006), Understanding the influence of Rossby waves on surface chlorophyll concentrations in the North Atlantic Ocean, *J. Mar. Res.*, *64*(1), 43–71.

Chavez, F. P., R. T. Barber, P. M. Kosro, A. Huyer, S. R. Ramp, T. P. Stanton, and B. R. Demendiola (1991), Horizontal transport and the distribution of nutrients in the coastal transition zone off Northern California: Effects on primary production, phytoplankton biomass and species composition, *J. Geophys. Res.*, *96*(C8), 14,833–14,848.

Chelton, D. B., and M. G. Schlax (1991), Estimation of time averages from irregularly spaced observations: With application to Coastal Zone Color Scanner estimates of chlorophyll concentration, *J. Geophys. Res.*, *96*(C8), 14,669–14,692.

Chelton, D. B., P. A. Bernal, and J. A. McGowan (1982), Large-scale interannual physical and biological interaction in the California current, *J. Mar. Res.*, *40*(4), 1095–1125.

Chereskin, T. K., M. Y. Morris, P. P. Niiler, P. M. Kosro, R. L. Smith, S. R. Ramp, C. A. Collins, and D. L. Musgrave (2000), Spatial and temporal characteristics of the mesoscale circulation of the California Current from eddy-resolving moored and shipboard measurements, *J. Geophys. Res.*, *105*(C1), 1245–1269.

Collins, C. A., L. M. Ivanov, O. V. Melnichenko, and N. Garfield (2004), California Undercurrent variability and eddy transport estimated from RAFOS float observations, *J. Geophys. Res.*, *109*, C05028, doi:10.1029/2003JC002191.

Cromwell, D. (2001), Sea surface height observations of the 34 degrees N 'waveguide' in the North Atlantic, *Geophys. Res. Lett.*, *28*(19), 3705–3708.

Daubechies, I. (1992), *Ten Lectures on Wavelet Analysis*, 357 pp., Soc. for Ind. and Appl. Math., Philadelphia, Pa.

Denman, K. L., and M. R. Abbott (1994), Time scales of pattern evolution from cross-spectrum analysis of advanced very high-resolution radiometer and coastal zone color scanner imagery, *J. Geophys. Res.*, *99*(C4), 7433–7442.

Durazo, R., et al. (2001), The state of the California Current, 2000–2001: A third straight La Niña year, *CalCOFI Rep.*, *42*, 29–60.

Francis, R. C., and S. R. Hare (1994), Decadal-scale regime shifts in the large marine ecosystems of the north–east Pacific: A case for historical science, *Fish. Oceanogr.*, *3*, 279–291.

Haidvogel, D. B., A. Beckmann, and K. S. Hedstrom (1991), Dynamic simulations of filament formation and evolution in the coastal transition zone, *J. Geophys. Res.*, *96*(C8), 15,017–15,040.

Haney, R. L., R. A. Hale, and D. E. Dietrich (2001), Offshore propagation of eddy kinetic energy in the California Current, *J. Geophys. Res.*, *106*(C6), 11,709–11,717.

Hayward, T. L., and A. W. Mantyla (1990), Physical, chemical and biological structure of a coastal eddy near Cape Mendocino, *J. Mar. Res.*, *48*(4), 825–850.

Hayward, T. L., et al. (1999), The state of the California Current in 1998–1999: Transition to cool-water conditions, *CalCOFI Rep.*, *40*, 29–62.

Henson, S. A., and A. C. Thomas (2007a), Phytoplankton scales of variability in the California Current System: 2. Latitudinal variability, *J. Geophys. Res.*, *112*, C07018, doi:10.1029/2006JC004040.

Henson, S. A., and A. C. Thomas (2007b), Interannual variability in timing of bloom initiation in the California Current System, *J. Geophys. Res.*, doi:10.1029/2006JC003960, in press.

Hickey, B. M. (1998), Coastal oceanography of western North America from the tip of Baja California to Vancouver Island, in *The Sea*, vol. 11, edited by A. R. Robinson and K. H. Brink, pp. 345–395, John Wiley, Hoboken, N. J.

Hood, R. R., M. R. Abbott, A. Huyer, and P. M. Kosro (1990), Surface patterns in temperature, flow, phytoplankton biomass and species composition in the coastal transition zone off northern California, *J. Geophys. Res.*, *95*(C10), 18,081–18,094.

Hood, R. R., M. R. Abbott, and A. Huyer (1991), Phytoplankton and photosynthetic light response in the coastal transition zone off northern California in June 1987, *J. Geophys. Res.*, *96*(C8), 14,769–14,780.

Huntley, M. E., M. Zhou, and W. Nordhausen (1995), Mesoscale distribution of zooplankton in the California Current in late spring, observed by optical plankton counter, *J. Mar. Res.*, *53*(4), 647–674.

Huyer, A., J. A. Barth, P. M. Kosro, R. K. Shearman, and R. L. Smith (1998), Upper-ocean water mass characteristics of the California Current, Summer 1993, *Deep Sea Res., Part II*, *45*(8–9), 1411–1442.

Ikeda, M., and W. J. Emery (1984), Satellite observations and modeling of meanders in the California Current System off Oregon and Northern California, *J. Phys. Oceanogr.*, *14*(9), 1434–1450.

Kahru, M., S. G. Marinone, S. E. Lluch-Cota, A. Pares-Siera, and B. G. Mitchell (2004), Ocean-color variability in the Gulf of California: scales from days to ENSO, *Deep Sea Res., Part II*, *51*(1–3), 139–146.

Kelly, K. A. (1985), The influence of winds and topography on the sea surface temperature patterns over the northern California slope, *J. Geophys. Res.*, *90*(C6), 11,783–11,798.

Kelly, K. A., R. C. Beardsley, R. Limeburner, K. H. Brink, J. D. Paduan, and T. K. Chereskin (1998), Variability of the near-surface eddy kinetic energy in the California Current based on altimetric, drifter and moored current data, *J. Geophys. Res.*, *103*(C6), 13,067–13,083.

Kosro, P. M. (1987), Structure of the coastal current field off northern California during the Coastal Ocean Dynamics Experiment, *J. Geophys. Res.*, *92*(C2), 1637–1654.

Kosro, P. M. (2003), Enhanced southward flow over the Oregon shelf in 2002: A conduit for subarctic water, *Geophys. Res. Lett.*, *30*(15), 8023, doi:10.1029/2003GL017436.

Kosro, P. M., W. T. Peterson, B. M. Hickey, R. K. Shearman, and S. D. Pierce (2006), The physical versus biological spring transition: 2005, *Geophys. Res. Lett.*, *33*, L22S03, doi:10.1029/2006GL027072.

Lau, K. M., and H. Weng (1995), Climate signal detection using wavelet transform: How to make a time series sing, *Bull. Am. Meteorol. Soc.*, *76*(12), 2391–2402.

Logerwell, E. A., and P. E. Smith (2001), Mesoscale eddies and survival of late stage Pacific sardine (*Sardinops sagax*) larvae, *Fish. Oceanogr.*, *10*(1), 13–25.

Lynn, R., and J. Simpson (1987), The California Current System: The seasonal variability of its physical characteristics, *J. Geophys. Res.*, *92*(C12), 12,947–12,966.

Lynn, R., et al. (1998), The state of the California current, 1997–1998: Transition to El Niño conditions, *CalCOFI Rep.*, *39*, 25–49.

Machu, E., B. Ferret, and V. Garcon (1999), Phytoplankton pigment distribution from SeaWiFS data in the subtropical convergence zone south of Africa: A wavelet analysis, *Geophys. Res. Lett.*, *26*(10), 1469–1472.

Mantua, N. J., and S. R. Hare (2002), The Pacific decadal oscillation, *J. Oceanogr.*, *58*(1), 35–44.

Mantua, N. J., S. R. Hare, Y. Zhang, J. M. Wallace, and R. C. Francis (1997), A Pacific interdecadal climate oscillation with impacts on salmon production, *Bull. Am. Meteorol. Soc.*, *78*(6), 1069–1079.

Marchesiello, P., J. C. McWilliams, and A. Shchepetkin (2003), Equilibrium structure and dynamics of the California Current System, *J. Phys. Oceanogr.*, *33*(4), 753–783.

McGowan, J. A., D. R. Cayan, and L. M. Dorman (1998), Climate-ocean variability and ecosystem response in the northeast Pacific, *Science*, *281*(5374), 210–217.

Meyers, S. D., B. G. Kelly, and J. J. O'Brien (1993), An introduction to wavelet analysis in oceanography and meteorology—With application to the dispersion of Yanai waves, *Mon. Weather Rev.*, *121*(10), 2858–2866.

Morlet, J. (1983), Sampling theory and wave propagation, in *Issues on Acoustic Signal/Image Processing and Recognition*, *NATO ASI Ser.*, vol. 1, edited by C. H. Chen, pp. 233–261, Springer, Berlin.

Murphree, T., S. J. Bograd, F. B. Schwing, and B. Ford (2003), Large scale atmosphere-ocean anomalies in the northeast Pacific during 2002, *Geophys. Res. Lett.*, *30*(15), 8026, doi:10.1029/2003GL017303.

Nezlin, N. P., and B. L. Li (2003), Time-series analysis of remote-sensed chlorophyll and environmental factors in the Santa Monica-San Pedro Basin off Southern California, *J. Mar. Syst.*, *39*(3–4), 185–202.

Nezlin, N. P., and J. C. McWilliams (2003), Satellite data, empirical orthogonal functions and the 1997–1998 El Niño off California, *Remote Sens. Environ.*, *84*(2), 234–254.

Pennington, J. T., K. L. Mahoney, V. S. Kuwahara, D. D. Kolber, R. Calienes, and F. P. Chavez (2006), Primary production in the eastern tropical Pacific: A review, *Prog. Oceanogr.*, *69*(2–4), 285–317.

Peterson, W. T., and F. B. Schwing (2003), A new climate regime in the northeast Pacific ecosystems, *Geophys. Res. Lett.*, *30*(17), 1896, doi:10.1029/2003GL017528.

Rienecker, M. M., and C. N. K. Mooers (1988), Mesoscale variability in current-meter measurements in the California Current System off Northern California, *J. Geophys. Res.*, *93*(C6), 6711–6734.

Sakuma, K. M., and S. Ralston (1997), Vertical and horizontal distribution of juvenile Pacific whiting (*Merluccius productus*) in relation to hydrography off California, *CalCOFI Rep.*, *38*, 137–146.

Schwing, F. B., C. S. Moore, S. Ralston, and K. M. Sakuma (2000), Record coastal upwelling in the California Current in 1999, *CalCOFI Rep.*, *41*, 148–160.

Schwing, F. B., et al. (2002a), The state of the California Current, 2001–2002: Will the California Current keep its cool, or is El Niño looming?, *CalCOFI Rep.*, *43*, 31–68.

Schwing, F. B., T. Murphree, L. deWitt, and P. M. Green (2002b), The evolution of oceanic and atmospheric anomalies in the Northeast Pacific during the El Niño and La Niña events of 1995–2000, *Prog. Oceanogr.*, *54*, 459–491.

Schwing, F. B., N. A. Bond, S. J. Bograd, T. Mitchell, M. A. Alexander, and N. Mantua (2006), Delayed coastal upwelling along the US West Coast in 2005: A historical perspective, *Geophys. Res. Lett.*, *33*, L22S01, doi:10.1029/2006GL026911.

Simpson, J. (1984a), El Niño induced onshore transport in the California current during 1982–1983, *Geophys. Res. Lett.*, *11*(3), 233–236.

Simpson, J. (1984b), A simple model of the 1982–83 Californian El Niño, *Geophys. Res. Lett.*, *11*(3), 237–240.

Smith, R. C., X. Y. Zhang, and J. Michaelsen (1998), Variability of pigment biomass in the California Current System as determined by satellite imagery: 1. Spatial variability, *J. Geophys. Res.*, *93*(D9), 10,863–10,882.

Soto-Mardones, L., A. Pares-Sierra, J. Garcia, R. Durazo, and S. Hormazabal (2004), Analysis of the mesoscale structure in the IMECOCAL region (off Baja California) from hydrographic, ADCP and altimetry data, *Deep Sea Res., Part II*, *51*(6–9), 785–798.

Spitz, Y. H., J. S. Allen, and J. Gan (2005), Modeling of ecosystem processes on the Oregon shelf during the 2001 summer upwelling, *J. Geophys. Res.*, *110*, C10S17, doi:10.1029/2005JC002870.

Strub, P. T., and C. James (1995), The large-scale summer circulation of the California Current, *Geophys. Res. Lett.*, *22*(3), 207–210.

Strub, P. T., and C. James (2000), Altimeter-derived variability of surface velocities in the California Current System: 2. Seasonal circulation and eddy statistics, *Deep Sea Res., Part II*, *47*(5–6), 831–870.

Strub, P. T., T. K. Chereskin, P. P. Niiler, C. James, and M. D. Levine (1997), Altimeter-derived variability of surface velocities in the California Current System: 1. Evaluation of TOPEX altimeter velocity resolution, *J. Geophys. Res.*, *102*(C6), 12,727–12,748.

Thomas, A. C., and P. Brickley (2006), Satellite measurements of chlorophyll distribution during spring 2005 in the California Current, *Geophys. Res. Lett.*, *33*(22), L22S05, doi:10.1029/2006GL026588.

Thomas, A. C., and P. T. Strub (1989), Interannual variability in phytoplankton pigment distribution during the spring transition along the west-coast of North America, *J. Geophys. Res.*, *94*(C12), 18,095–18,117.

Thomas, A. C., and P. T. Strub (2001), Cross-shelf phytoplankton pigment variability in the California Current, *Cont. Shelf Res.*, *21*(11–12), 1157–1190.

Thomas, A. C., P. T. Strub, and P. Brickley (2003), Anomalous satellite-measured chlorophyll concentrations in the northern California Current in 2001–2002, *Geophys. Res. Lett.*, *30*(15), 8022, doi:10.1029/2003GL017409.

Thomson, R. E., M. C. Healey, J. F. T. Morris, and G. A. Borstad (1992), Commercial troll fishing vessel distribution off Vancouver Island during July 1988—Relation to observed physical oceanography, *Can. J. Fish. Aquat. Sci.*, *49*(4), 820–832.

Torrence, C., and G. P. Compo (1998), A practical guide to wavelet analysis, *Bull. Am. Meteorol. Soc.*, *79*(1), 61–78.

Tynan, C. T., D. G. Ainley, J. A. Barth, T. J. Cowles, S. D. Pierce, and L. B. Spear (2005), Cetacean distributions relative to ocean processes in the northern California Current System, *Deep Sea Res., Part II*, *52*(1–2), 145–167.

Venrick, E., et al. (2003), The state of the California Current, 2002–2003: Tropical and subarctic influences vie for dominance, *CalCOFI Rep.*, *44*, 28–60.

Wang, B., and Y. Wang (1996), Temporal structure of the Southern Oscillation as revealed by waveform and wavelet analysis, *J. Clim.*, *9*(7), 1586–1598.

Wheeler, P., A. Huyer, and J. Fleischbein (2003), Cold halocline, increased nutrients and higher chlorophyll off Oregon in 2002, *Geophys. Res. Lett.*, *30*(14), 8021, doi:10.1029/2003GL017395.

S. A. Henson and A. C. Thomas, School of Marine Sciences, University of Maine, Orono, ME 04469, USA. (stephanie.henson@umit.maine.edu)